CHIN. PHYS. LETT. Vol. 38, No. 10 (2021) 107401 **Express Letter**

# High $T_c$ Superconductivity in Heavy Rare Earth Hydrides

Hao Song(宋昊)[1], Zihan Zhang(张子涵)[1], Tian Cui(崔田)[2,1*], Chris J. Pickard[3,4], Vladimir Z. Kresin[5], and Defang Duan(段德芳)[1*]

[1]*State Key Laboratory of Superhard Materials, College of Physics, Jilin University, Changchun 130012, China*
[2]*Institute of High Pressure Physics, School of Physical Science and Technology, Ningbo University, Ningbo 315211, China*
[3]*Department of Materials Science & Metallurgy, University of Cambridge, 27 Charles Babbage Road, Cambridge CB3 0FS, United Kingdom*
[4]*Advanced Institute for Materials Research, Tohoku University 2-1-1 Katahira, Aoba, Sendai, 980-8577, Japan*
[5]*Lawrence Berkeley Laboratory, University of California at Berkeley, Berkeley, CA 94720, USA*

(Received 20 August 2021; accepted 2 September 2021; published online 8 September 2021)

Sulfur and lanthanum hydrides under compression display superconducting states with high observed critical temperatures. It has been recently demonstrated that carbonaceous sulfur hydride displays room temperature superconductivity. However, this phenomenon has been observed only at very high pressure. Here, we theoretically search for superconductors with very high critical temperatures, but at much lower pressures. We describe two of such sodalite-type clathrate hydrides, $YbH_6$ and $LuH_6$. These hydrides are metastable and are predicted to superconduct with $T_c \sim 145$ K at 70 GPa and $T_c \sim 273$ K at 100 GPa, respectively. This striking result is a consequence of the strong interrelationship between the $f$ states present at the Fermi level, structural stability, and the final $T_c$ value. For example, $TmH_6$, with unfilled $4f$ orbitals, is stable at 50 GPa, but has a relatively low value of $T_c$ of 25 K. The $YbH_6$ and $LuH_6$ compounds, with their filled $f$-shells, exhibit prominent phonon "softening", which leads to a strong electron-phonon coupling, and as a result, an increase in $T_c$.

DOI: 10.1088/0256-307X/38/10/107401

It has been predicted for a long time that metallic monoatomic hydrogen under high pressure enters a superconducting state, with a high value of critical temperature $T_c$.[1] However, very high pressures are required to observe this phenomenon; and it has yet to be realized.[2–7] A promising route to room temperature superconductivity is to study hydrogen-rich compounds (or hydrides). Because of chemical precompression effects, they metallize at lower pressures,[8] see reviews.[9–11] The presence of two ions, light (e.g., H) and heavy, in the unit cell, leads to an appearance of optical high frequency phonon modes (vibrations of H ions) with a large phonon density of states (DOS) across the whole range of phonon momenta. This increases the magnitude of the electron-phonon interaction. An additional contribution due to the heavy ions (acoustic modes) further increases the electron-phonon interaction. Among such hydrides are $H_3S$[12,13] and $LaH_{10}$,[14,15] for which high $T_c$ values were predicted and later confirmed experimentally.[16–20] These materials display values of $T_c$ exceeding 200 K at pressures above 150 GPa. Recently, it has been reported that the compound of hydrogen, carbon and sulfur displays the transition at 288 K,[21] that is, at room temperature. However, because the high pressures require ($267 \pm 10$ GPa), the observation and corresponding analysis are rather difficult, so are practical or technological applications.

The observation of high temperature superconductivity in the hydrides requires pressures as high as 150 GPa. The next frontier is observation of room-temperature superconductivity at significantly lower pressures (with a clear final goal of reaching ambient pressure). In this Letter, we present a step in this direction. Indeed, it will be demonstrated that high values of $T_c$ are expected to be observed in $YbH_6$ with $T_c \sim 145$ K at 70 GPa and, most strikingly, in $LuH_6$ with $T_c \sim 273$ K at 100 GPa.

Given the large number of superconducting hydrides,[9–11,22] now it is time to develop general concepts and define major factors that favor high values of $T_c$. Tm, Yb, and Lu occupy special positions among rare earth (RE) elements. Yb has filled $4f$ orbital with the configuration $4f^{14}$ and does not display ferromagnetic or antiferromagnetic order. Its electronegativity is 1.1, similar to those of Ca and Y. It exhibits a mixed valence and is a superconductor at high pressure.[23] Adjacent to ytterbium, thulium has $13e$ filled $4f$ orbitals with $4f^{13}$. Lutetium has filled $4f$ orbital and an extra $5d$ electron with $4f^{14}5d^1$, and it is the hard-

Supported by the National Natural Science Foundation of China (Grant Nos. 12122405, 51632002, and 11974133), the Program for Changjiang Scholars and Innovative Research Team in Universities (Grant No. IRT_15R23). C.J.P. acknowledges financial support from the Engineering and Physical Sciences Research Council (Grant No. EP/P022596/1).
*Corresponding authors. Email: cuitian@nbu.edu.cn; duandf@jlu.edu.cn
© 2021 Chinese Physical Society and IOP Publishing Ltd

est and most dense metal among the RE elements. The $f$ electrons in the hydrides containing these elements are expected to affect superconductivity and structural stability. We will discuss the corresponding role of the $f$ states in these superconducting hydrides in detail below.

As is well-known, on-site Coulomb interactions are particularly significant for localized $f$ electrons. We first evaluate the equation of state (EOS) for $YbH_2$. Then we compare it with the experimental EOS to assess the reliability of our DFT calculations (see Fig. S1). For the high-pressure phase $P6_3/mmc$ of $YbH_2$, the ultra-soft pseudo-potentials at the DFT level provides a good agreement between the theory and experiment (the detailed discussion is in the Supplementary Materials). Furthermore, we construct the high-pressure phase diagram of the Yb–H system with both DFT and DFT+$U$ ($U = 5$ eV), through extensive structure searches via the *ab initio* random structure searching method as implemented in the AIRSS code.[24,25] The results are presented in Fig. S2. One can see that the convex hull is essentially unchanged between DFT+$U$ and DFT. In addition, we calculate $T_c$ of Yb at DFT level and find that $T_c$'s are 1.6 K at 86 GPa and 4.6 K at 180 GPa. There is a good agreement between our calculation and the experimental measurements[23] (1.4 K at 86 GPa and 4.6 K at 179 GPa). Therefore, we consider that the DFT level calculations for the Yb–H system above 50 GPa are acceptable.

Combining the convex hull (Fig. S2), enthalpy differences (Fig. S3) and phonon dispersion (Figs. S4 and S5) of the Yb–H system under high pressure, we construct the pressure-composition phase diagram in Fig. 1(a). Note that eight stoichiometries YbH, $YbH_2$, $Yb_2H_5$, $YbH_3$, $YbH_4$, $YbH_6$, $YbH_8$ and $YbH_{12}$ are stable over different pressure ranges. The crystal structures of our predicted stable Yb hydrides are shown in Fig. S6; the lattice parameters are provided in Table S1. For YbH, the $Fm\bar{3}m$ phase, with hydrogens occupying octahedral interstices, transforms into a $Cmcm$ phase at 170 GPa. $YbH_2$ adopts the space group $P6_3/mmc$ at low pressure, which is consistent with the experimental measurements.[26] We find that it transforms to a $P6/mmm$ phase at 233 GPa. $R\bar{3}m$-$Yb_2H_5$ is stable between 145 and 250 GPa. $YbH_3$ favors an $Fm\bar{3}m$ structure below 145 GPa, the hydrogen atoms occupy both octahedral and tetrahedral interstices. $YbH_4$ maintains the space group $I4/mmm$ isotypic with $CaH_4$[27] and $YH_4$[28] in the pressure range of 70–300 GPa, which contains monatomic H and molecular $H_2$. $YbH_8$ with $P6_3/mmc$ symmetry is stable above 240 GPa; as determined by the phonon dispersion (see Fig. S5). The high hydrogen content $YbH_{12}$, with $R\bar{3}$ symmetry, is stable in the pressure range of 70–240 GPa.

For the case of $YbH_6$, it has two phases of $C2/m$ and $Im\bar{3}m$, and the phase transition occurs at 158 GPa. The $Im\bar{3}m$ phase contains clathrate $H_{24}$ cage and consists of eight $H_6$ hexagons and six $H_4$ squares. It is isostructural with $Im\bar{3}m$ $CaH_6$[27] and $YH_6$,[28] which have been synthesized at high pressure to exhibit high $T_c$ of 215 K and 224 K, respectively.[29,30] Electron localization functions (ELF) of cubic $YbH_6$ show weak covalent interaction between the H atoms, with an ELF of 0.58 (see Fig. 1(c) and Fig. S7). The high pressure phase diagram and crystal structure of the Yb–H system are very similar to the Ca–H and Y–H systems. Therefore, they could have similar properties, such as high-temperature superconductivity.

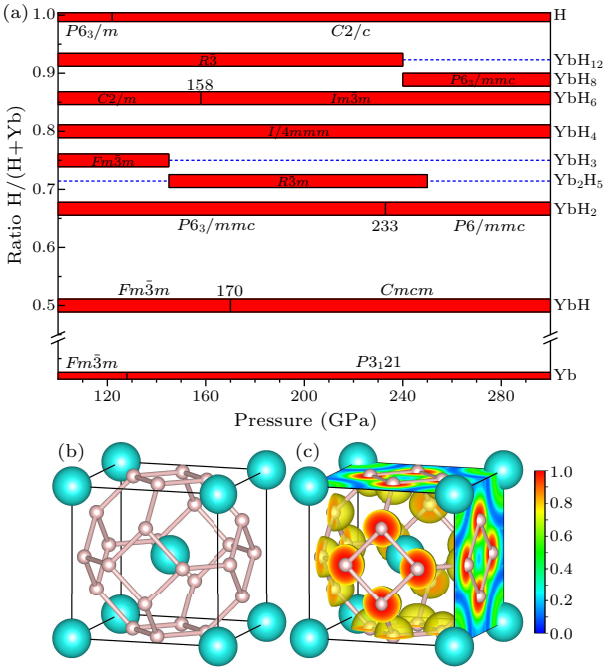


**Fig. 1.** (a) Pressure-composition phase diagram of the Yb–H system. [(b), (c)] The crystal structures and electron localization functions (ELFs) of $Im\bar{3}m$-$YbH_6$. The large cyan balls and small pink balls represent ytterbium and hydrogen, respectively.

Structure searches for the other two heavy rare earth (RE = Tm, Lu) hydrides adjacent to Yb were also performed using AIRSS.[24,25] The resulting convex hull diagrams at different pressures are shown in Fig. S8. We also find that cubic $TmH_6$ and $LuH_6$ are located on the convex hull at 200 and 400 GPa, respectively, indicating that they are thermodynamically stable at these pressures. Combining enthalpy differences and phonon dispersions of the Tm–H and Lu–H systems under high pressures, we find that the cubic $TmH_6$ and $LuH_6$ are stable above 130 GPa and 370 GPa, respectively. The lattice parameters of predicted stable Tm–H and Lu–H compounds are provided in Table S2.

We calculate the electronic properties of $Im\bar{3}m$-$YbH_6$, as shown in Fig. 2(a). Remarkably, the $4f$ or-

bitals associated with the Yb atom form a set of localized and almost non-dispersive bands that appear about 1 eV below the Fermi level. To gain an insight into the role of the $f$ electrons in the heavy rare earth (RE = Tm, Yb, Lu) sodalite-like hydrides, we calculate the band structure and density of electronic states of $TmH_6$ and $LuH_6$ at 100 GPa. Compared with $YbH_6$ and $LuH_6$, $TmH_6$ has unfilled $4f$ orbitals. We can see that the $f$ electrons of $TmH_6$ dominate the Fermi level [see Fig. 2(b)]. For $LuH_6$, the fully filled $4f$ orbitals and one extra electron in the $5d$ orbitals leads to the $4f$ electrons moving downwards in the band structure [see Fig. 2(c)]. In addition, we investigate magnetic properties for $TmH_6$, $YbH_6$ and $LuH_6$ at the pressure range of 50 to 150 GPa in Fig. 2(d). The results show that $YbH_6$ and $LuH_6$ are nonmagnetic, while $TmH_6$ is magnetic, and the strength of magnetism decreases with increasing pressure [see Fig. 2(d)]. The Mulliken population scheme[31] provides a qualitative analysis on atomic charge, bond population, charge transfer. At 100 GPa, electrons of $YbH_6$ transfer from $4f$ orbitals of Yb to $1s$ orbital of H by $0.34|e|$ ($e$ being the elementary charge). In $YbH_6$, the $4f$ orbitals of Yb thus remain nearly fully filled (e.g., 13.66 out of $14|e|$), exhibiting no local magnetism. Electrons also transfer from Yb $6s$ and $5p$ orbitals to Yb $5d$ orbitals and H $s$ orbitals. In summary, Yb atoms play the role of electron donors and each of them loses approximately $1.0|e|$; each H uniformly gains $\frac{1}{6}|e|$. The electron transfer in $TmH_6$ is very similar to that in $YbH_6$. Tm transfers about $1.0|e|$ to H atoms, but unfilled $4f$ orbitals have less electrons of $12.86|e|$ resulting in magnetic moment of $\sim 1.2\mu_B$ at 100 GPa. For $LuH_6$, there is almost no electron transfer out of the $4f$ orbitals, but as compared to $YbH_6$ and $TmH_6$, three electrons transfer from Lu $6s$ and $5d$ orbitals to hydrogen atoms.

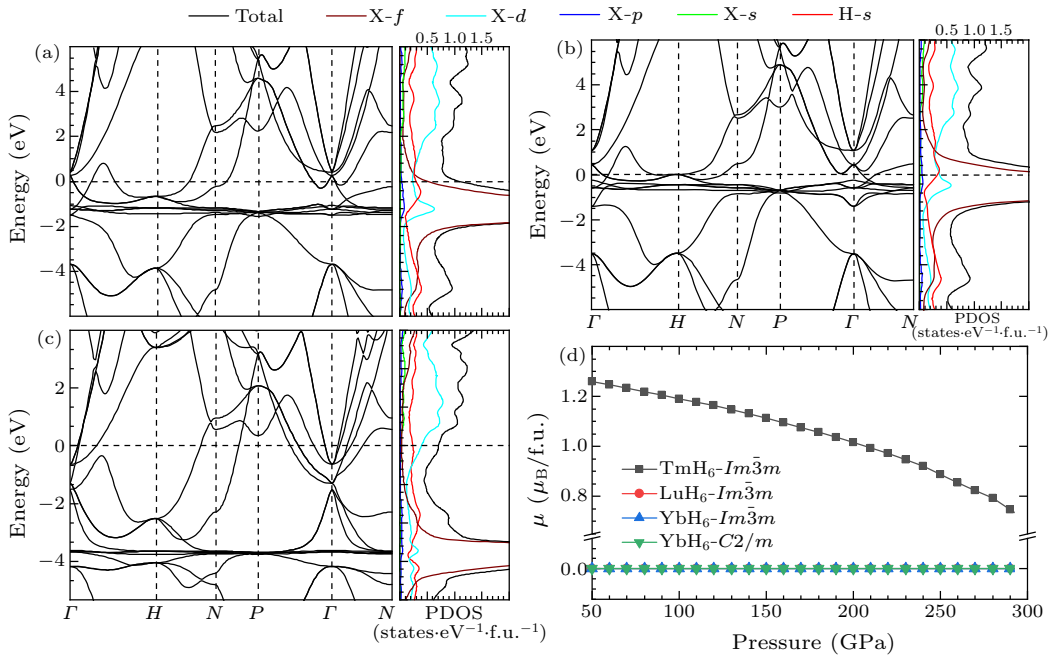


**Fig. 2.** Band structure and projected density of electronic states (PDOS) of (a) $YbH_6$, (b) $TmH_6$ and (c) $LuH_6$ at 100 GPa. (d) Magnetic moments of $XH_6$ (X = Tm, Yb, Lu) compounds at high pressure.

Generally, the high $T_c$ superconducting state of the hydrides is created by strong electron-phonon coupling (EPC) to high frequency optical phonons (see, e.g., Refs. [12,14,32,33]). Firstly, we calculate the phonon spectrum for $Im\bar{3}m$-$YbH_6$ at 70 GPa and 200 GPa, for $TmH_6$ at 50 GPa and for $LuH_6$ at 100 GPa (Fig. 3). The absence of any imaginary frequency indicates their dynamical stability. It is notable that $YbH_6$ is dynamically stable down to relatively low pressures (70 GPa). The phonon modes are separated into two parts: the acoustic phonon modes (low frequencies $<220\,cm^{-1}$) dominated by vibrations of Yb atoms and the optical phonon modes (high frequencies) from the vibrations of H atoms. For $YbH_6$, the EPC parameter $\lambda$ is 2.2 at 70 GPa, and the optical phonon modes contribute to 90% of the total $\lambda$. As shown in Fig. 3(a), a striking feature of the phonon spectrum for $YbH_6$ is the presence of soft phonon modes along $\Gamma$–$H$ and $H$–$N$ directions. However, with increasing pressure from 70 to 100 GPa, phonon branches rapidly harden and the EPC parameter $\lambda$ substantially decreases from 2.2 to 1.3, which lead to a large reduction of $T_c$ from 145 to 116 K (see Fig. S9). We can see that the phonon softening at 70 GPa does boost the EPC strength. The phonon dispersion and EPC parameter $\lambda$ of $TmH_6$ and $LuH_6$ are also calculated [see Figs. 3(c) and 3(d)]. It is shown that the EPC parameter $\lambda$ of $TmH_6$ is 0.72, optical phonon modes contribute to 84% of the

total $\lambda$; as for the critical temperature $T_c$, it is only 25 K. In sharp contrast, $LuH_6$ is dynamically stable at 100 GPa, and its EPC parameter $\lambda$ is 3.60, optical phonon modes contribute to 85% of the total $\lambda$, yield a high $T_c = 273$ K. Moreover, several phonon branches show significant phonon softening and it is clearly seen that $\lambda_{q,v}$ is enhanced in these regions of phonon softening. The critical temperatures of the remaining predicted stable Lu–H compounds are calculated, for example, $LuH_5$ is superconducting with $T_c \sim 89$ K at 150 GPa, see detail in Table S4. In each case, the EPC parameter $\lambda$ decreases with increasing pressure. The values of $T_c$ for $TmH_6$, $YbH_6$ and $LuH_6$, mentioned above, are estimated with use of self-consistent iterations (IA) for solution of the Eliashberg equations, as shown in Fig. S11. We also calculate the critical temperature using the Allen–Dynes-modified McMillan equation (Mc-A-D) and the Gor'kov–Kresin equation (G-K). The obtained values of $T_c$ appear to be slightly lower than those obtained with IA, see Table S3.

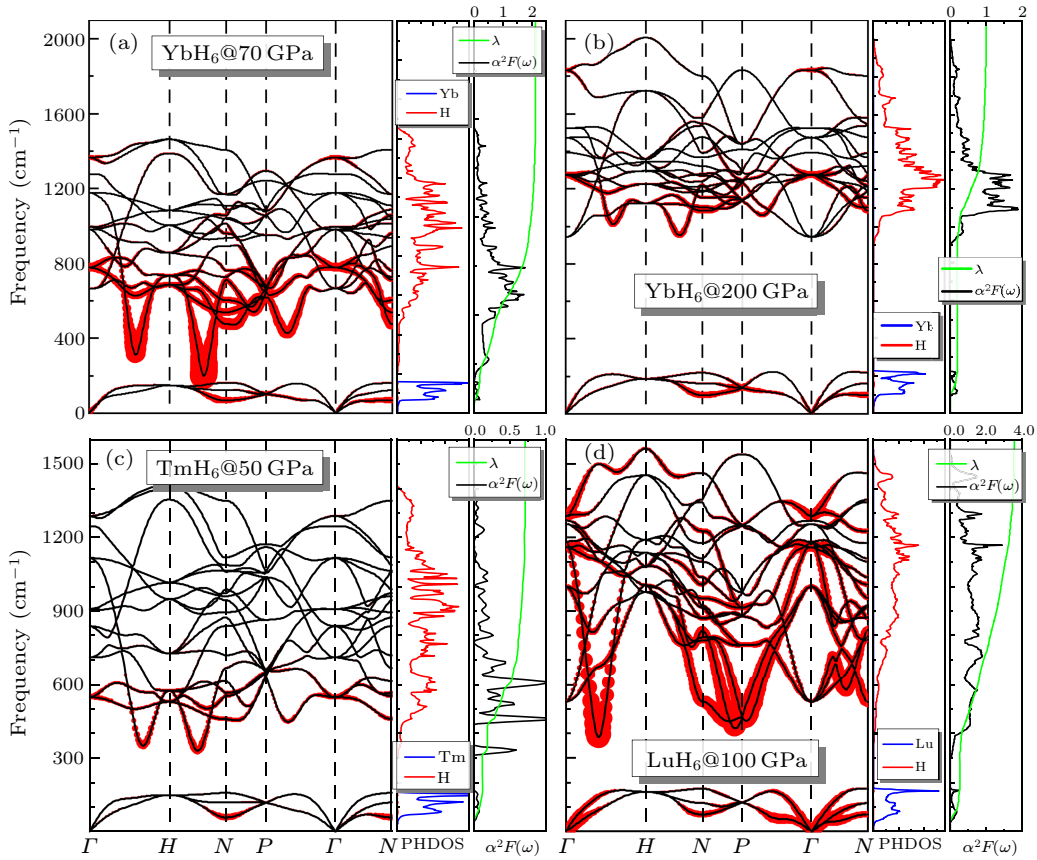


**Fig. 3.** Phonon dispersion, phonon density of state, spectral function $\alpha^2F(\omega)$ and integral EPC $\lambda$ of $Im\bar{3}m$-$YbH_6$ (a) at 70 GPa and (b) 200 GPa, $TmH_6$ (c) at 50 GPa, $LuH_6$ (d) at 100 GPa. Red circles show mode-resolved electron-phonon coupling constants $\lambda_{q,v}$ and the radius of the circles are proportional to the EPC strength.

The value of the isotope coefficient for the H→D substitutions directly reflects to the interplay between the optical and acoustic phonon modes. We calculate the isotope coefficient for cubic $XH_6$ hydrides (X = Yb, Lu, Tm, Ca, Sc, Y) using the two-coupling constants method[34] [see Eq. (S10)]. One can see that the isotope coefficients for cubic lanthanide hydrides are large and close to the optimum value ($\alpha_{max} = 0.5$), see Fig. 4. Such large values reflect the dominant contribution of the optical modes (see Table S3). As for $CaH_6$ and $ScH_6$, the values of isotope coefficients are also large, while smaller than $YbH_6$ and $LuH_6$. They are comparable with those for $H_3S$, see Refs. [34,35]. The critical temperature of $XD_6$ ($T_c^D$) was estimated according to the equation of $T_c/T_c^D = (M_D/M_H)^\alpha$, where $T_c$ is obtained from the G-K equation (see Table S5).

We now focus on the impact of the $f$ states upon the superconducting properties. It is noted that highly localized $f$ electrons in RE hydrides affect superconductivity adversely.[15,36] For example, according to experimental observations at high pressure, $LaH_{10}$ and $CeH_9$ have high $T_c$ of 250–160 K and 117 K, respectively, while $T_c$'s of $PrH_9$[37] and $NdH_9$[38] are found to be as low as 10 K. It is interesting that the value of the critical temperature for RE hydrides grad-

ually decreases with an increase in filling of the $f$-shell and superconductivity disappears for the compound $EuH_9$ with half-filled $f$-shells (Eu-$f^7$).[39]

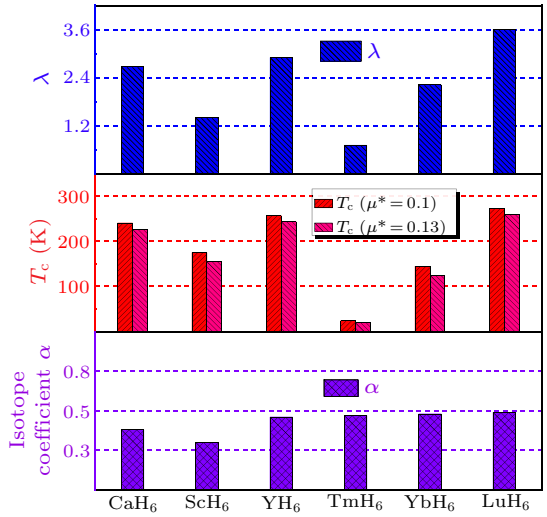


**Fig. 4.** Superconductivity critical temperature $T_c$ and EPC parameter $\lambda$ of various clathrate hydrides at high pressures. The pressure values are 150, 120, 50, 70 and 100 GPa for $CaH_6$, $YH_6$, $TmH_6$, $YbH_6$ and $LuH_6$, respectively.

As mentioned above, we study various compositions of $XH_n$ (X = Tm, Yb, Lu). The most interesting hydrides at high pressure are the $TmH_6$, $YbH_6$, and $LuH_6$ compounds. They are dynamically stable at 50 GPa, 70 GPa and 100 GPa with $T_c$ of 25 K, 145 K and 273 K (ice point temperature), respectively. We uncover a non-trivial and non-monotonic dependence of $T_c$ on the degree of the $f$-shell filling. Beyond filling half of the $f$-shell, the $T_c$ of heavy RE hydrides gradually increases upon further filling. It reaches a maximum in the last RE hydrides $LuH_6$, which is comparable with $LaH_{10}$. Importantly, the pressure providing the dynamical stability for $LuH_6$ is much lower than that for $LaH_{10}$ (171 GPa for experimental observation and 210 GPa for predictions in the harmonic approximation). As a result, one can expect that the superconducting state of $LuH_6$ with values of $T_c$ that are close to room temperature can be observed at much lower pressure.

To gain more insight into the correlation between the presence of the $f$ states, stability, and the value of $T_c$, we compute the phonon dispersion and EPC in an extreme case of freezing the $f$ manifold, through the Yb pseudopotential (see Fig. S10). The frozen-$f$ calculations show that the cubic structure becomes dynamically stable just above 100 GPa; as for the EPC, the parameter $\lambda$ is approximately equal to 5.5; then $T_c = 262$ K with $\mu^* = 0.1$. An increase in pressure leads to sharp decrease in the value of the EPC parameter $\lambda$ ($\lambda = 2.2$ at 200 GPa), but $\lambda$ is still more than two times larger compared to its value in the presence of $f$ electrons. One can conclude that the presence of the $f$ electrons in valence state leads to suppression of the phonon "softening". The dynamical stability of structure is enhanced, but the strength of the EPC is reduced. Therefore, the presence of the $f$ electronic states at the Fermi surface increases the dynamical stability but reduces the superconducting $T_c$.

The hydride $LuH_6$, with filled $4f$ orbitals and $1e$ filled $5d$ valence orbitals, is a remarkable compound with the highest $T_c$ among other cubic $XH_6$ (see Fig. 4); its $T_c$ value is comparable with that of the $LaH_{10}$ ($T_c = 250$–$260$ K, La also has $1e$ filled $5d$ orbitals). Moving from the light to heavy RE, one can observe that $T_c$ initially decreases and then gradually increases upon further filling of the $f$-shells above its half filling. Finally, it reaches a maximum $T_c$ for the last RE hydride, $LuH_6$.

It has been a long-term goal to obtain high-temperature superconductors in hydrides at pressures below 100 GPa. Here, we report a prediction of the realization of this dream in $YbH_6$ and $LuH_6$ compounds. As mentioned above, multi-megabar pressures are currently required to force the hydrides into the superconducting states to achieve high $T_c$. However, there should be a compromise and balance between the value of $T_c$ and the required pressure. One can propose the figure of merit $S$ (see Eq. (8) in Ref. [40]), which makes the compromise explicit. Lower values of both $S(H_3S)$ and $S(LaH_{10})$ equal to 1.3 reflect the very high pressures required to achieve the superconducting states. As for our results, $S(YbH_6) = 1.8$ and $S(LuH_6) = 2.5$; both values exceed those for $S(H_3S)$ and $S(LaH_{10})$. When we plot these $S$ values and pressures in figure of merit $S$ (see Fig. S12 and Fig. 10 in Ref. [40]), we find that $LuH_6$ sits somewhere between the iron based superconductors and the cuprates.

In summary, we have investigated the heavy RE hydrides, in particular those with the sodalite hydrogen cage structure, at high pressure. The temperature of the transition into the superconducting state correlates strongly with the presence of $f$ states at the Fermi level. For example, the $TmH_6$ compound is stable at low pressure (50 GPa), whereas its $T_c$ is relatively low ($T_c = 25$ K). One predicts much higher $T_c$ for $YbH_6$ ($T_c = 145$ K at 70 GPa). The optimal case corresponds to $LuH_6$. Remarkably, the critical temperature for this compound is predicted to reach $T_c = 273$ K at $P = 100$ GPa. Such a pressure is much below those required for other high $T_c$ hydrides. One may speculate that cubic clathrate ternary hydrides doped with heavy RE elements Yb and Lu could be synthesized at much lower pressure, exhibiting high temperature superconducting states.

*Acknowledgement.* We thank Professor Hanyu Liu and Professor Hongjian Zhao for interesting and stimulating discussions. Parts of the calculations were performed in the High Performance Computing Center of

Jilin University and on TianHe-1(A) at the National Supercomputer Center in Tianjin.

## References


[1] Ashcroft N W 1968 *Phys. Rev. Lett.* **21** 1748
[2] Mao H K and Hemley R J 1994 *Rev. Mod. Phys.* **66** 671
[3] Loubeyre P, Occelli F and LeToullec R 2002 *Nature* **416** 613
[4] Huang X, Li F, Huang Y, Wu G, Li X, Zhou Q, Liu B and Cui T 2016 *Chin. Phys. B* **25** 037401
[5] Dalladay-Simpson P, Howie R T and Gregoryanz E 2016 *Nature* **529** 63
[6] Dias R P and Silvera I F 2017 *Science* **355** 715
[7] Monserrat B, Drummond N D, Dalladay-Simpson P, Howie R T, López R P, Gregoryanz E, Pickard C J and Needs R J 2018 *Phys. Rev. Lett.* **120** 255701
[8] Ashcroft N W 2004 *Phys. Rev. Lett.* **92** 187002
[9] Duan D F, Liu Y X, Ma Y B, Shao Z, Liu B B and Cui T 2017 *Natl. Sci. Rev.* **4** 121
[10] Duan D F, Yu H Y, Xie H and Cui T 2019 *J. Supercond. Novel Magn.* **32** 53
[11] Bi T, Zarifi N, Terpstra T and Zurek E 2019 *Reference Module in Chemistry, Molecular Sciences and Chemical Engineering* (Amsterdam: Elsevier) pp 1–36
[12] Duan D F, Liu Y, Tian F, Li D, Huang X, Zhao Z, Yu H, Liu B, Tian W and Cui T 2015 *Sci. Rep.* **4** 6968
[13] Duan D F, Huang X, Tian F, Li D, Yu H, Liu Y, Ma Y, Liu B and Cui T 2015 *Phys. Rev. B* **91** 180502(R)
[14] Liu H, Naumov I I, Hoffmann R, Ashcroft N W and Hemley R J 2017 *Proc. Natl. Acad. Sci. USA* **114** 6990
[15] Peng F, Sun Y, Pickard C J, Needs R J, Wu Q and Ma Y 2017 *Phys. Rev. Lett.* **119** 107001
[16] Somayazulu M, Ahart M, Mishra A K, Geballe Z M, Baldini M, Meng Y, Struzhkin V V and Hemley R J 2019 *Phys. Rev. Lett.* **122** 027001
[17] Drozdov A P, Kong P P, Minkov V S, Besedin S P, Kuzovnikov M A, Mozaffari S, Balicas L, Balakirev F F, Graf D E, Prakapenka V B, Greenberg E, Knyazev D A, Tkacz M and Eremets M I 2019 *Nature* **569** 528
[18] Einaga M, Sakata M, Ishikawa T, Shimizu K, Eremets M I, Drozdov A P, Troyan I A, Hirao N and Ohishi Y 2016 *Nat. Phys.* **12** 835
[19] Drozdov A P, Eremets M I, Troyan I A, Ksenofontov V and Shylin S I 2015 *Nature* **525** 73
[20] Hong F, Yang L, Shan P, Yang P, Liu Z, Sun J, Yin Y, Yu X, Cheng J and Zhao Z 2020 *Chin. Phys. Lett.* **37** 107401
[21] Snider E, Dasenbrock-Gammon N, McBride R, Debessai M, Vindana H, Vencatasamy K, Lawler K V, Salamat A and Dias R P 2020 *Nature* **586** 373
[22] Ma J, Kuang J, Cui W, Chen J, Gao K, Hao J, Shi J and Li Y 2021 *Chin. Phys. Lett.* **38** 027401
[23] Song J, Fabbris G, Bi W, Haskel D and Schilling J S 2018 *Phys. Rev. Lett.* **121** 037004
[24] Pickard C J and Needs R J 2011 *J. Phys.: Condens. Matter* **23** 053201
[25] Pickard C J and Needs R J 2006 *Phys. Rev. Lett.* **97** 045504
[26] Olsen J S, Buras B, Gerward L, Johansson B, Lebech B, Skriver H L and Steenstrup S 1984 *Phys. Scr.* **29** 503
[27] Wang H, John S T, Tanaka K, Iitaka T and Ma Y 2012 *Proc. Natl. Acad. Sci. USA* **109** 6463
[28] Li Y, Hao J, Liu H, Tse J S, Wang Y and Ma Y 2015 *Sci. Rep.* **5** 9948
[29] Ma L, Wang K, Xie Y, Yang X, Wang Y, Zhou M, Liu H, Liu G, Wang H and Ma Y 2021 arXiv:2103.16282 [cond-mat.supr-con]
[30] Troyan I A, Semenok D V, Kvashnin A G, Sadakov A V, Sobolevskiy O A, Pudalov V M, Ivanova A G, Prakapenka V B, Greenberg E, Gavriliuk A G *et al.* 2021 *Adv. Mater.* **33** 2006832
[31] Segall M D, Shah R, Pickard C J and Payne M C 1996 *Phys. Rev. B* **54** 16317
[32] Song H, Duan D, Cui T and Kresin V Z 2020 *Phys. Rev. B* **102** 014510
[33] Xie H, Yao Y, Feng X, Duan D, Song H, Zhang Z, Jiang S, Redfern S A T, Kresin V Z, Pickard C J and Cui T 2020 *Phys. Rev. Lett.* **125** 217001
[34] Gor'kov L P and Kresin V Z 2018 *Rev. Mod. Phys.* **90** 011001
[35] Gor'kov L P and Kresin V Z 2016 *Sci. Rep.* **6** 7
[36] Semenok D V, Kruglov I A, Savkin I A, Kvashnin A G and Oganov A R 2020 *Curr. Opin. Solid State Mat. Sci.* **24** 100808
[37] Zhou D, Semenok D, Duan D, Xie H, Huang X, Chen W, Li X, Liu B, Oganov A R and Cui T 2020 *Sci. Adv.* **6** eaax6849
[38] Zhou D, Semenok D V, Xie H, Huang X L, Duan D F, Aperis A, Oppeneer P M, Galasso M, Kartsev A I, Kvashnin A G, Oganov A R and Cui T 2020 *J. Am. Chem. Soc.* **142** 2803
[39] Semenok D V, Zhou D, Kvashnin A G, Huang X, Galasso M, Kruglov I A, Ivanova A G, Gavriliuk A G, Chen W, Tkachenko N V, Boldyrev A I, Troyan I, Oganov A R and Cui T 2021 *J. Phys. Chem. Lett.* **12** 32
[40] Pickard C J, Errea I and Eremets M I 2020 *Annu. Rev. Condens. Matter Phys.* **11** 57

# Supplementary Materials for "High $T_c$ superconductivity in Heavy Rare Earth hydrides"

Hao Song(宋昊)[1], Zihan Zhang(张子涵)[1], Tian Cui(崔田)[2,1,*], Chris J. Pickard[3,4], Vladimir Z. Kresin[5], Defang Duan(段德芳)[1,†]

[1]*State Key Laboratory of Superhard Materials, College of Physics, Jilin University, Changchun 130012, China*

[2]*Institute of High Pressure Physics, School of Physical Science and Technology, Ningbo University, Ningbo 315211, China*

[3]*Department of Materials Science & Metallurgy, University of Cambridge, 27 Charles Babbage Road, Cambridge CB3 0FS, United Kingdom*

[4]*Advanced Institute for Materials Research, Tohoku University 2-1-1 Katahira, Aoba, Sendai, 980-8577, Japan*

[5]*Lawrence Berkeley Laboratory, University of California at Berkeley, Berkeley, CA 94720, USA*

Corresponding authors email: *cuitian@nbu.edu.cn

Corresponding authors email: †duandf@jlu.edu.cn

# Content

**1. Computational method ..... S2**
**2. The reliability of DFT calculations ..... S3**
**3. Convex hull diagram of Yb-H ..... S4**
**4. Structural parameters, enthalpy difference curves and phonon dispersion of Yb-H ..... S5**
**5. Electronic properties of $YbH_6$ ..... S9**
**6. Convex hull diagram of Lu-H and Tm-H ..... S10**
**7. Equations for calculating $T_c$ and related parameters ..... S12**
**8. Superconductive properties ..... S16**
**References ..... S22**

## 1. Computational method

For the structure searching we used the *ab initio* random structure searching (AIRSS) approach method [1,2] and the underlying energetic simulations were performed with the CASTEP code [3-5]. The ultrasoft pseudopotentials [6] with the valence electrons Yb ($5s^2 5p^6 4f^{14} 6s^2$), Tm ($5s^2 5p^6 4f^{13} 6s^2$), Lu ($5s^2 5p^6 4f^{14} 5d^1 6s^2$) and H ($1s^1$), Perdew-Burke-Ernzerhof generalized gradient approximation [7], a plane-wave cutoff of 400 eV and Monkhorst-Pack meshes [8] *k*-point spacing of $2\pi \times 0.07$ Å$^{-1}$ were used in these searches. Extensive structure searches were performed at 100, 200 and 300 GPa with 1 to 24 hydrogen atoms and 1-4 ytterbium atoms, each structure search at fixed pressure yielded about 7000 structures. Then we re-optimized the structures on the convex hull with high accuracy parameters (a plane-wave cutoff of 700 eV and Monkhorst-Pack meshes *k*-point spacing of $2\pi \times 0.03$ Å$^{-1}$ were used) to re-confirm the convex hull. Structure searches for Tm-H and Lu-H system were also performed by AIRSS code. Phonon spectra and electron–phonon coupling (EPC) were studied in the framework of density-functional perturbation theory implemented in the Quantum ESPRESSO package [9]. Ultrasoft pseudopotentials were used with a kinetic energy cutoff of 80 Ry. We adopted $18 \times 18 \times 18$ k-points grid and $6 \times 6 \times 6$ q-points for $Im\bar{3}m$-$YbH_6$. The superconducting transition temperatures $T_c$ are evaluated with use of the Eliashberg equation [10] with a Coulomb pseudopotential $\mu^*$=0.1-0.13. We employed three different methods: the Allen−Dynes-modified McMillan equation (Mc-A-D) with correction factors [11]; an approach with self-consistent iterations (IA) [11-13], and the Gor'kov-Kresin theory (G-K) [14].

## 2. The reliability of DFT calculations

We first evaluated the equation of state (EOS) for $YbH_2$. Then it was compared with the experimental EOS to assess the reliability of our DFT calculations (see Fig. S1). One can see that for the low-pressure phase *Pnma* of $YbH_2$, calculations using the on the fly pseudo-potentials poorly reproduce the experimental EOS; there is a significant volume discrepancy at the same pressure. The ultra-soft pseudo-potentials calculations substantially improve the agreement with the experiment; the agreement is further improved with the DFT+U scheme. One can see that there is a good agreement between the theory and experiment for the high-pressure phase $P6_3/mmc$ of $YbH_2$, if we use the ultra-soft pseudo-potentials scheme. The authors of previous work concerned with ytterbium hydrides [15], used a Hubbard U = 5 eV for lower pressure phases and U= 0 eV for high-pressure phases to reproduce available experimental data, in clear agreement with our results (see Fig. S1).

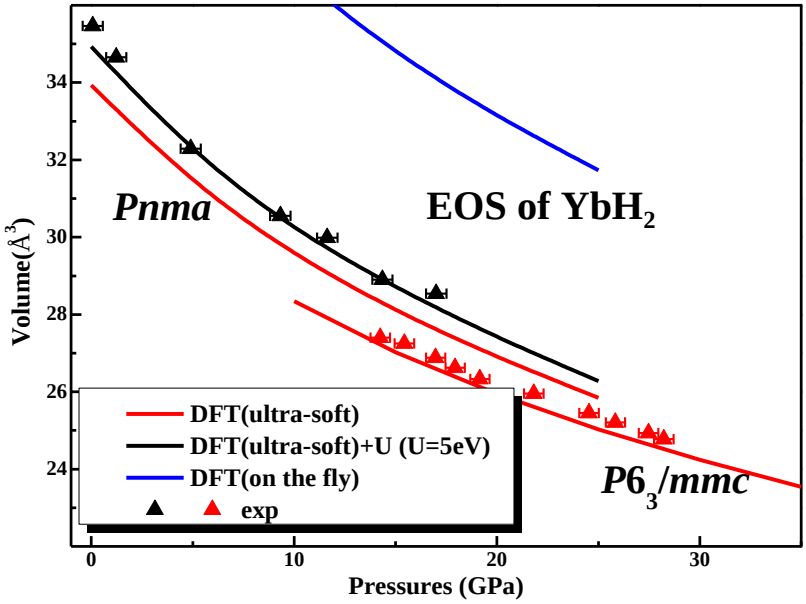


**Fig. S1.** Volumes as a function of pressures for low pressure phase *Pnma* and high pressure phase $P6_3/mmc$ for $YbH_2$ calculated using the DFT with ultra-soft (red line) and on the fly potentials (blue line), DFT with ultra-soft potentials plus Hubbard repulsion (DFT+U, black line), and compared with experiment for $YbH_2$ [16] (solid triangle).

## 3. Convex hull diagram of Yb-H

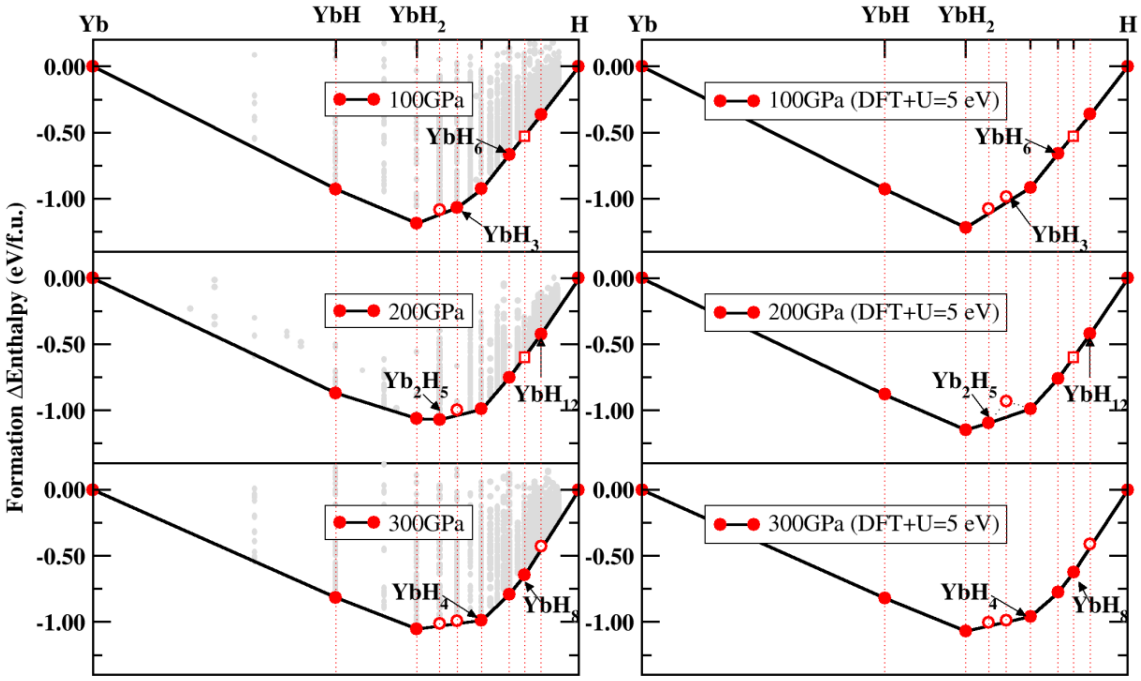


**Fig. S2.** Convex hull of the Yb-H without and with DFT+U (U=5 eV) at 100, 200 and 300 GPa. The solid circle, open circle and open square symbols indicate that the structures are thermodynamic stable, thermodynamic unstable and dynamic unstable, respectively. As can be seen, DFT+U slightly changes the convex-hull. With DFT+U, $YbH_3$ is off the convex hull at 100 GPa; without DFT+U, $YbH_3$ is off the convex hull at 200 GPa.

## 4. Structural parameters, enthalpy difference curves and phonon dispersion of Yb-H

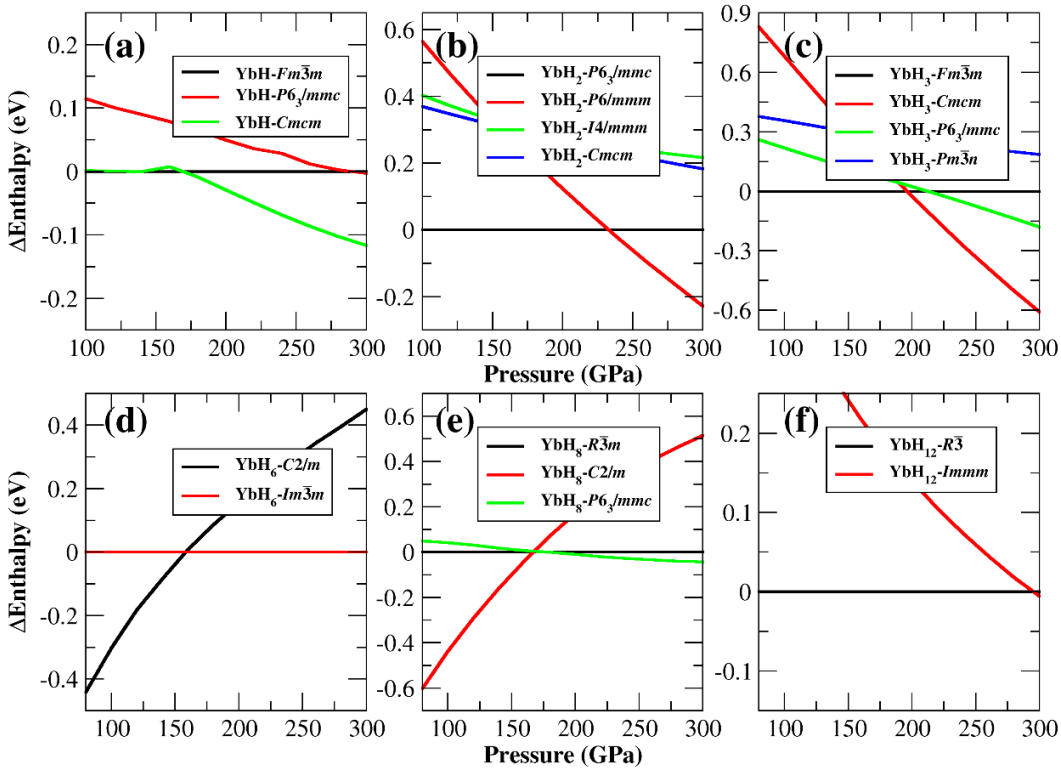


**Fig. S3.** The enthalpy difference ($\Delta H$) curves of $YbH_n$ (n=1, 2, 3, 6, 8 and 12) from 100 to 300 GPa.

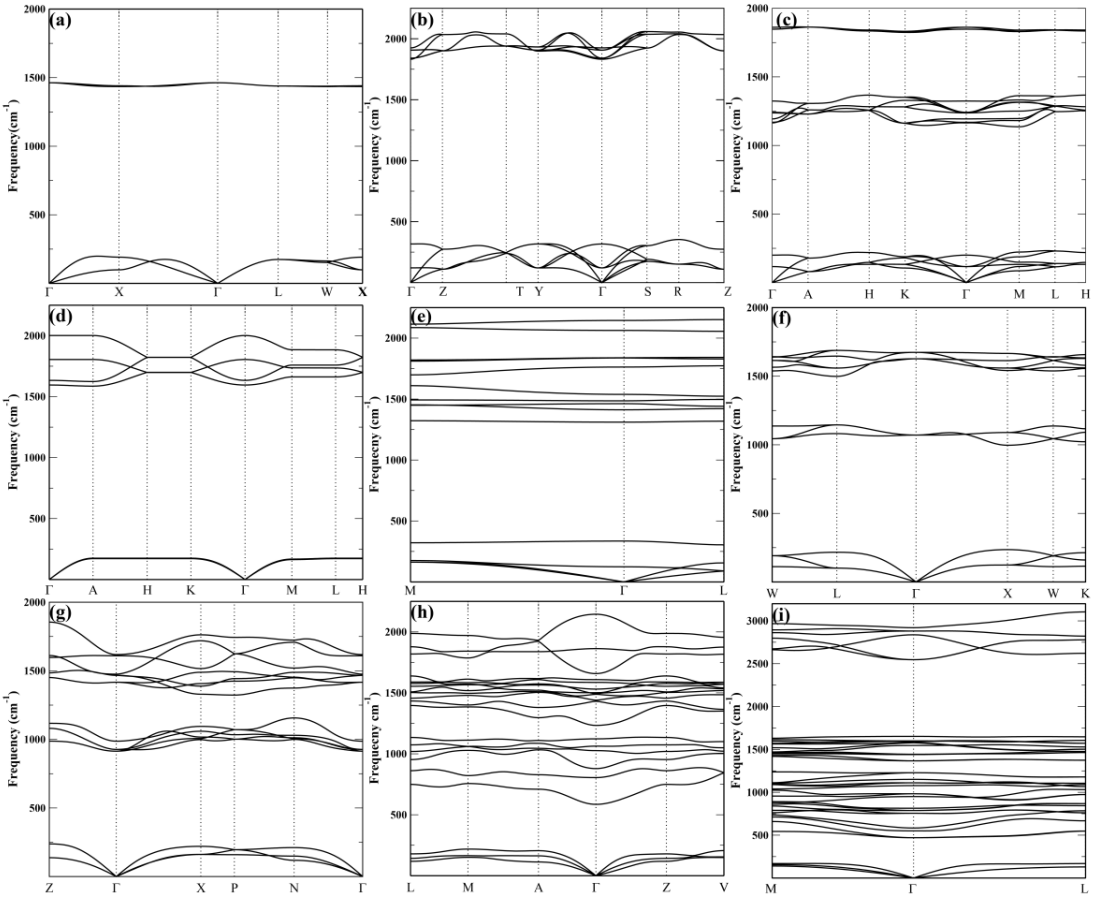


**Fig. S4.** Phonon dispersion of (a) $Fm\bar{3}m$-YbH at 100 GPa, (b) *Cmcm*-YbH at 250 GPa, (c) $P6_3/mmc$-$YbH_2$ at 100 GPa, (d) $P6/mmm$-$YbH_2$ at 300 GPa, (e) $R\bar{3}m$-$Yb_2H_5$ at 200 GPa, (f) $Fm\bar{3}m$-$YbH_3$ at 100 GPa, (g) $I4/mmm$-$YbH_4$ at 100 GPa, (h) $C2/m$ $YbH_6$ at 100 GPa, (i) $R\bar{3}$-$YbH_{12}$ at 100 GPa.

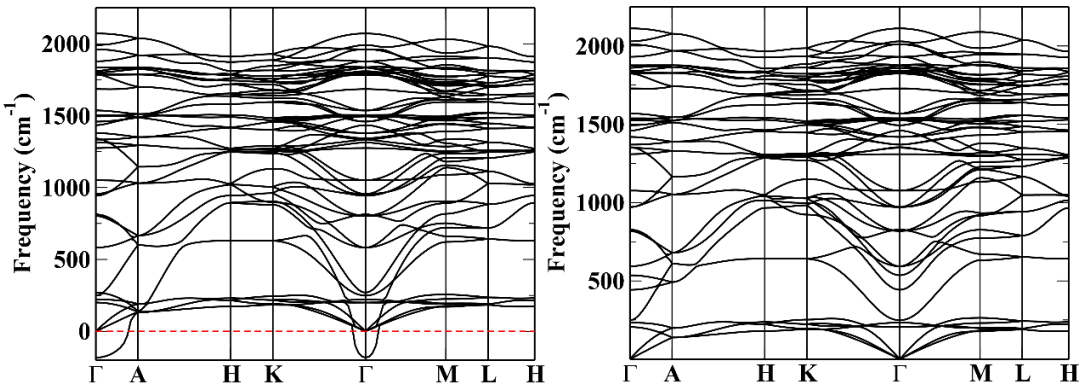


**Fig. S5.** Phonon dispersion of $P6_3/mmc$-$YbH_8$ at 220 GPa (left) and 240 GPa (right).

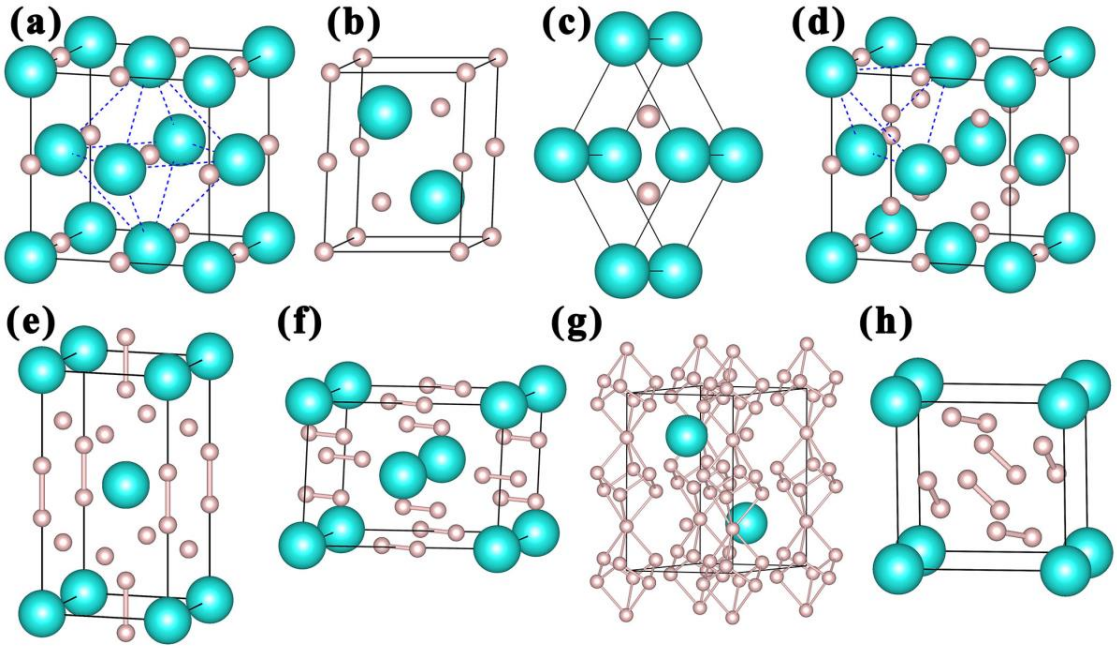


**Fig. S6.** The crystal structures of ytterbium hydrides (a) $Fm\bar{3}m$-YbH, (b) $P6_3/mmc$-$YbH_2$, (c) $P6/mmm$-$YbH_2$, (d) $Fm\bar{3}m$-$YbH_3$, (e) $I4/mmm$-$YbH_4$, (f) $C2/m$-$YbH_6$, (g) $P6_3/mmc$-$YbH_8$, (h) $R\bar{3}$-$YbH_{12}$.

**Table S1.** Calculated structural parameters of stable and metastable $YbH_n$ (n=1-12) compounds.

| | Space group | Lattice parameters (Å) | Atoms | Atomic coordinates (fractional) | | |
|---|---|---|---|---|---|---|
| | | | | X | Y | Z |
| YbH (100 GPa) | $Fm\bar{3}m$ | $a$=$b$=$c$= 4.01<br>$\alpha$ =$\beta$ =$\gamma$ =90° | H(4b)<br>Yb(4a) | 0.50<br>0.00 | 0.50<br>0.00 | 0.50<br>0.00 |
| YbH (200 GPa) | *Cmcm* | $a$= 3.74<br>$b$= 3.88<br>$c$= 3.57<br>$\alpha$ =$\beta$ =$\gamma$ =90° | H(4c)<br>Yb(4c) | 0.50<br>0.50 | 0.33<br>0.20 | 0.25<br>0.75 |
| $YbH_2$ (100 GPa) | $P6_3/mmc$ | $a$=$b$=3.22<br>$c$= 4.10<br>$\alpha$ =$\beta$ =$\gamma$ =90° | H(2d)<br>H(2a)<br>Yb(2c) | 1/3<br>0.00<br>2/3 | 2/3<br>0.00<br>1/3 | 0.75<br>0.00<br>0.75 |
| $YbH_2$ (300 GPa) | *P6/mmm* | $a$=$b$=2.52<br>$c$= 2.33<br>$\alpha$ =$\beta$ =90°<br>$\gamma$ =120° | H(2d)<br>Yb(1a) | 2/3<br>0.00 | 1/3<br>0.00 | 0.50<br>0.00 |
| $YbH_3$ (100 GPa) | $Fm\bar{3}m$ | $a$=$b$=$c$= 4.36<br>$\alpha$ =$\beta$ =$\gamma$ =90° | H(8c)<br>H(4b)<br>Yb(4a) | 0.25<br>0.50<br>0.00 | 0.25<br>0.50<br>0.00 | 0.25<br>0.50<br>0.00 |
| $YbH_4$ (120 GPa) | *I4/mmm* | $a$=$b$=2.84<br>$c$ = 5.12<br>$\alpha$ =$\beta$ =$\gamma$ =90° | H(4d)<br>H(4e)<br>Yb(2a) | 0.50<br>0.50<br>0.00 | 0.00<br>0.50<br>0.00 | 0.25<br>0.094<br>0.00 |
| $YbH_6$ (100 GPa) | *C*2/*m* | $a$ = 5.14<br>$b$ = 3.80<br>$c$ = 3.04<br>$\alpha$ =$\gamma$ =90° $\beta$ =119° | H(8j)<br>H(4i)<br>Yb(2a) | 0.11<br>0.61<br>0.00 | -0.29<br>0.00<br>0.00 | 0.59<br>0.09<br>0.00 |
| $YbH_6$ (70 GPa) | $Im\bar{3}m$ | $a$=$b$=$c$=3.79<br>$\alpha$ =$\beta$ =$\gamma$ =90° | H(12d)<br>Yb(2a) | 0.25<br>0.00 | 0.00<br>0.00 | 0.50<br>0.00 |
| $YbH_6$ (200 GPa) | $Im\bar{3}m$ | $a$=$b$=$c$=3.47<br>$\alpha$ =$\beta$ =$\gamma$ =90° | H(12d)<br>Yb(2a) | 0.25<br>0.00 | 0.00<br>0.00 | 0.50<br>0.00 |
| $YH_6$ [17] (200 GPa) | $Im\bar{3}m$ | $a$=$b$=$c$=3.53<br>$\alpha$ =$\beta$ =$\gamma$ =90° | H(12d)<br>Yb(2a) | 0.25<br>0.00 | 0.00<br>0.00 | 0.50<br>0.00 |
| $CaH_6$ [18] (150 GPa) | $Im\bar{3}m$ | $a$=$b$=$c$=3.50<br>$\alpha$ =$\beta$ =$\gamma$ =90° | H(12d)<br>Yb(2a) | 0.25<br>0.00 | 0.00<br>0.00 | 0.50<br>0.00 |

| | | | | | | |
|---|---|---|---|---|---|---|
| $YbH_8$ (300 GPa) | $P6_3/mmc$ | $a=b=3.10$<br>$c=5.07$<br>$\alpha=\beta=90°$<br>$\gamma=120°$ | H(12k)<br>H(2d)<br>H(2b)<br>Yb(2c) | 0.16<br>2/3<br>0.00<br>2/3 | 0.33<br>1/3<br>0.00<br>1/3 | 0.94<br>0.25<br>0.25<br>0.75 |
| $YbH_{12}$ (200 GPa) | $R\bar{3}$ | $a=b=4.44$<br>$c=5.52$<br>$\alpha=\beta=90°$<br>$\gamma=120°$ | H(18f)<br>H(18f)<br>Yb(3a) | 0.24<br>-0.17<br>0.00 | 0.25<br>-0.71<br>0.00 | -0.56<br>0.03<br>0.00 |

## 5. Electronic properties of $YbH_6$

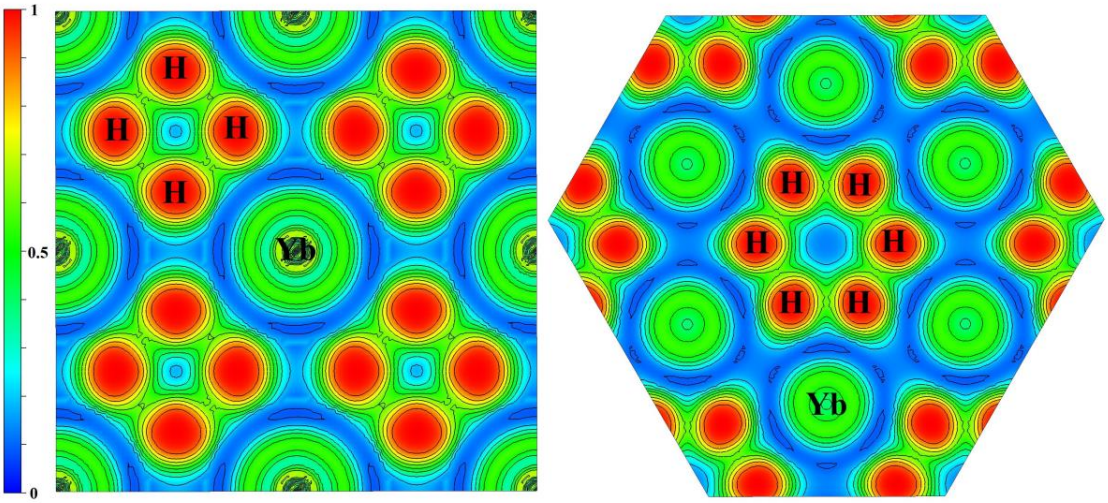


**Fig. S7.** The electron localization functions (ELF) of cubic $YbH_6$ at 70 GPa for [0 0 1] plane (left panel) and [1 1 -1] plane (right panel). The isopleth curves are plotted with interval 0.1.

## 6. Convex hull diagram of Lu-H and Tm-H

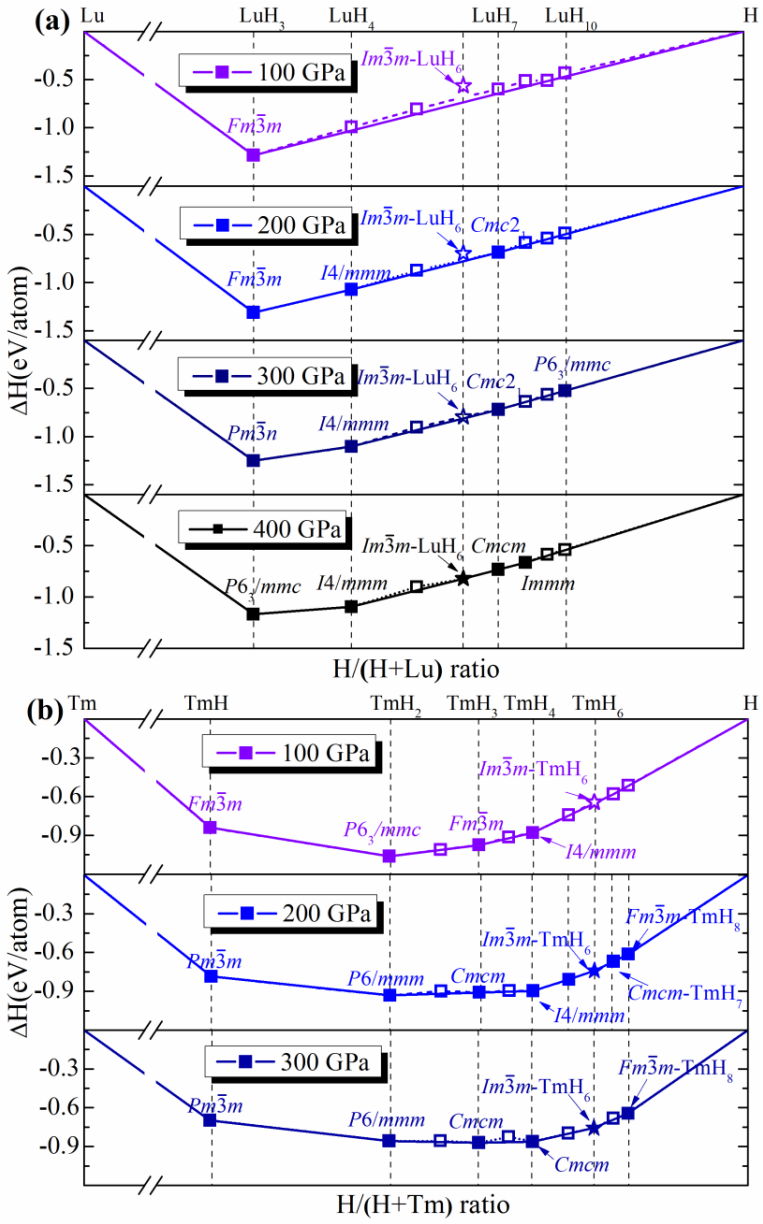


**Fig. S8.** Convex hull of (a) Lu-H at 100, 200, 300, and 400 GPa, (b) Tm-H at 100, 200 and 300 GPa. The solid and open symbols indicate that the structures are thermodynamic stable and unstable, respectively. The open stars indicate the cubic $LuH_6$ (10 meV above the convex hull at 300 GPa) and $TmH_6$ (8 meV above the convex hull at 100 GPa).

**Table S2.** Calculated structural parameters of Lu-H and Tm-H compounds.

| | Space group | Lattice parameters (Å) | Atoms | Atomic coordinates (fractional) | | |
|---|---|---|---|---|---|---|
| | | | | X | Y | Z |
| $LuH_3$ (100 GPa) | $Fm\bar{3}m$ | $a=b=c=4.35$ $\alpha=\beta=\gamma=90°$ | H(8c) | 0.25 | 0.25 | 0.25 |
| | | | H(4b) | 0.50 | 0.50 | 0.50 |
| | | | Lu(4a) | 0.00 | 0.00 | 0.00 |
| $LuH_4$ (100 GPa) | $I4/mmm$ | $a=b=3.56$ $c=3.13$ $\alpha=\beta=\gamma=90°$ | H(8j) | 0.20 | 0.50 | 0.00 |
| | | | Lu(2a) | 0.00 | 0.00 | 0.00 |
| $LuH_5$ (200 GPa) | $P4/nmm$ | $a=b=3.43$ $c=3.55$ $\alpha=\beta=\gamma=90°$ | H(2b) | 0.50 | 0.50 | 0.50 |
| | | | H(8i) | 0.50 | 0.74 | 0.80 |
| | | | Lu(2c) | 0.00 | 0.50 | 0.74 |
| $LuH_6$ (100 GPa) | $Fm\bar{3}m$ | $a=b=c=3.69$ $\alpha=\beta=\gamma=90°$ | H(8c) | 0.25 | 0.25 | 0.25 |
| | | | H(4b) | 0.50 | 0.50 | 0.50 |
| | | | Lu(4a) | 0.00 | 0.00 | 0.00 |
| $LuH_7$ (150 GPa) | $Cmc2_1$ | $a=3.27$ $b=5.50$ $c=5.60$ $\alpha=\beta=\gamma=90°$ | H(8b) | 0.74 | 0.09 | 0.14 |
| | | | H(8b) | 0.71 | 0.04 | 0.72 |
| | | | H(4a) | 0.50 | 0.19 | 0.63 |
| | | | H(4a) | 0.50 | 0.99 | 0.93 |
| | | | H(4a) | 0.50 | 0.68 | 0.85 |
| | | | Lu(4a) | 0.50 | 0.33 | 0.93 |
| TmH (50 GPa) | $Fm\bar{3}m$ | $a=b=c=4.24$ $\alpha=\beta=\gamma=90°$ | H(4b) | 0.50 | 0.50 | 0.50 |
| | | | Tm(4a) | 0.00 | 0.00 | 0.00 |
| $TmH_2$ (50 GPa) | $P6_3/mmc$ | $a=b=2.39$ $c=4.39$ $\alpha=\beta=\gamma=90°$ | H(2d) | 1/3 | 2/3 | 0.75 |
| | | | H(2a) | 0.00 | 0.00 | 0.00 |
| | | | Tm(2c) | 2/3 | 1/3 | 0.75 |
| $TmH_3$ (50 GPa) | $Fm\bar{3}m$ | $a=b=c=4.58$ $\alpha=\beta=\gamma=90°$ | H(8c) | 0.25 | 0.25 | 0.25 |
| | | | H(4b) | 0.50 | 0.50 | 0.50 |
| | | | Tm(4a) | 0.00 | 0.00 | 0.00 |
| $TmH_4$ (50 GPa) | $I4/mmm$ | $a=b=3.08$ $c=5.40$ $\alpha=\beta=\gamma=90°$ | H(4d) | 0.50 | 0.00 | 0.25 |
| | | | H(4e) | 0.50 | 0.50 | 0.094 |
| | | | Tm(2a) | 0.00 | 0.00 | 0.00 |
| $TmH_6$ (50 GPa) | $Fm\bar{3}m$ | $a=b=c=3.85$ $\alpha=\beta=\gamma=90°$ | H(8c) | 0.25 | 0.25 | 0.25 |
| | | | H(4b) | 0.50 | 0.50 | 0.50 |
| | | | Tm(4a) | 0.00 | 0.00 | 0.00 |

## 7. Equations for calculating $T_c$ and related parameters

### (1) Self-consistent iteration solution of the Eliashberg equation

The Eliashberg equation has a form[10,19,20]:

$$\Delta(i\omega_n)Z(i\omega_n) = \frac{\pi T}{N_F}\sum_{n'}\frac{\Delta(i\omega_n')}{\sqrt{\omega_n'^2+\Delta^2(i\omega_n')}} \times [\lambda(\omega_n - \omega_{n'}) - N_F\mu^*]\delta(\epsilon) \quad \text{(S1)}$$

$$Z(i\omega_n) = 1 + \frac{\pi T}{N_F\omega_n}\sum_{n'}\frac{\omega_n'}{\sqrt{\omega_n'^2+\Delta^2(i\omega_n')}}\lambda(\omega_n - \omega_{n'})\delta(\epsilon) \quad \text{(S2)}$$

Here functions $\Delta(i\omega_n)$ and $Z(i\omega_n)$ represent pairing order parameter and the renormalization function, $N_F$ is the density of electronic states at the Fermi level, and $\delta(\epsilon)$ is the Dirac delta function. $i\omega_n = i(2n+1)\pi T_c$ are the fermion Matsubara frequencies (we employ the themodynamic Green's functions formalism (see,e.g.,[21]); $\mu^*$ is the Coulomb pseudopotential, for which we use the widely accepted range of 0.1-0.13. $\lambda(\omega_n - \omega_{n'})$ contains the electron-phonon coupling matrix, phonon propagator. and the phonon density of states, and is given by:

$$\lambda(\omega_n - \omega_{n'}) = \int_0^\infty d\omega \frac{2\omega}{(\omega_n-\omega_n')^2+\omega^2}\alpha^2F(\omega) \quad \text{(S3)}$$

The equations for the order parameter and the renormalization function form a coupled nonlinear system and are solved self-consistently. We evaluated the renormalization function and the order parameter for each Matsubara frequency along the imaginary energy axis. After calculating $Z(i\omega_n)$ and $\Delta(i\omega_n)$, an analytic continuation is performed to the real axis using the Pade' functions.The calculation is performed for each T ($T_{min}<T\leq T_{max}$) ($T_{min}\approx 0$ and $T_{max}\geq T_c$). The critical temperature $T_c$ is obtained as an asymptotic value as $\Delta(i\omega_n)$ tends to zero.

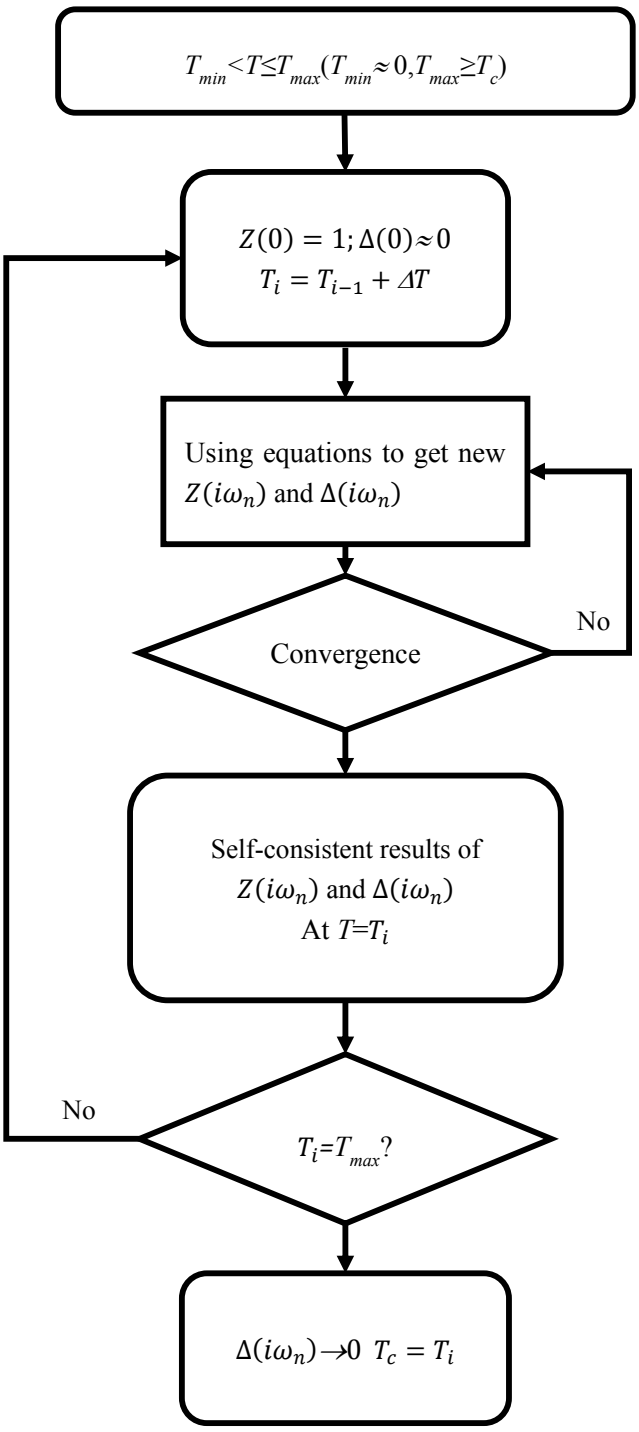
$T_{min}<T\leq T_{max}(T_{min}\approx 0, T_{max}\geq T_c)$
$Z(0)=1;\Delta(0)\approx 0$
$T_i = T_{i-1} + \Delta T$
Using equations to get new $Z(i\omega_n)$ and $\Delta(i\omega_n)$
Convergence
No
Self-consistent results of $Z(i\omega_n)$ and $\Delta(i\omega_n)$ At $T=T_i$
$T_i=T_{max}$?
No
$\Delta(i\omega_n)\to 0$ $T_c = T_i$

**(2) The McMillan−Allen−Dynes equation**

The McMillan−Allen−Dynes equation (Mc-A-D) is the approximate analytic solution of the Eliashberg equations at λ < 1.5; it has a form [11]:

$$T_c = \frac{\omega_{log}}{1.2}\exp\left[-\frac{1.04(1+\lambda)}{\lambda-\mu^*(1+0.62\lambda)}\right], \quad \text{(S4)}$$

If λ > 1.5, one should use the more general equation containing the corrections $f_1$ and $f_2$ :

$$T_c = \frac{f_1 f_2 \omega_{log}}{1.2}\exp\left[-\frac{1.04(1+\lambda)}{\lambda-\mu^*(1+0.62\lambda)}\right], \quad \text{(S5)}$$

where $f_1$ and $f_2$ are given by [11]:

$$f_1 = \sqrt[3]{\left[1+\left(\frac{\lambda}{2.46(1+3.8\mu^*)}\right)^{\frac{3}{2}}\right]}, f_2 = 1+\frac{(\frac{\bar{\omega}_2}{\omega_{log}}-1)\lambda^2}{\lambda^2+[1.82(1+6.3\mu^*)\frac{\bar{\omega}_2}{\omega_{log}}]^2}, \quad \text{(S6)}$$

Here $\bar{\omega}_2$ is themean square frequency,

$$\bar{\omega}_2 = \sqrt{\frac{2}{\lambda}\int \alpha^2F(\omega)\,\omega d\omega}\,, \quad \text{(S7)}$$

$\omega_{log}$ is the logarithmic average frequency. The $\omega_{log}$ and EPC constant λ are defined by the relations:

$$\omega_{log} = \exp\left[\frac{2}{\lambda}\int \frac{d\omega}{\omega}\alpha^2F(\omega)\ln\omega\right], \quad \text{(S8)}$$

$$\lambda = 2\int \frac{\alpha^2\mathrm{F}(\omega)}{\omega}d\omega, \quad \text{(S9)}$$

**(3) Gor'kov-Kresin equation**

Gor'kov and Kresin (G-K) introduced the coupling constants $\lambda_{opt}$ and $\lambda_{ac}$ describing the interaction of electrons with optical and acoustic phonons[14,22]. The generalized Eliashberg equation has the form (at $T$=$T_c$):

$$\Delta(\omega_n)Z = \pi T\sum_{\omega_{n'}}\left[\lambda_{\mathrm{opt}}\frac{\widetilde{\Omega}^2_{\mathrm{opt}}}{\widetilde{\Omega}^2_{\mathrm{opt}}+(\omega_n-\omega_{n'})^2}+\lambda_{\mathrm{ac}}\frac{\widetilde{\Omega}^2_{\mathrm{ac}}}{\widetilde{\Omega}^2_{\mathrm{ac}}+(\omega_n-\omega_{n'})^2}\right]\frac{\Delta(\omega_{n'})}{|\omega_{n'}|}_{|T=T_c}, \quad \text{(S10)}$$

$$\lambda_{\mathrm{ac}} = 2\int_0^{\Omega_1}\frac{\alpha^2F(\omega)}{\omega}d\omega,\ \lambda_{\mathrm{opt}} = 2\int_{\Omega_1}^{\Omega_m}\frac{\alpha^2F(\omega)}{\omega}d\omega,\ \lambda_{\mathrm{ac}}+\lambda_{\mathrm{opt}} = \lambda, \quad \text{(S11)}$$

where $\omega_1$ is the maximum frequency for the acoustic modes, $\omega_m$ is the maximum frequency's value. The mean square average frequency values are defined as follows:

$$\widetilde{\omega}_{\mathrm{ac}} = \langle {\omega_{\mathrm{ac}}}^2 \rangle^{\frac{1}{2}}, \langle {\omega_{\mathrm{ac}}}^2 \rangle = \frac{2}{\lambda_{\mathrm{ac}}} \int_0^{\omega_1} d\omega \cdot \omega^2 \frac{\alpha^2 F(\omega)}{\omega} = \frac{2}{\lambda_{\mathrm{ac}}} \int_0^{\omega_1} \alpha^2 F(\omega) \omega d\omega, \quad \text{(S12)}$$

$$\widetilde{\omega}_{\mathrm{opt}} = \langle {\omega_{\mathrm{opt}}}^2 \rangle^{\frac{1}{2}}, \langle {\omega_{\mathrm{opt}}}^2 \rangle = \frac{2}{\lambda_{\mathrm{opt}}} \int_{\omega_1}^{\omega_{\mathrm{m}}} d\omega \cdot \omega^2 \frac{\alpha^2 F(\omega)}{\omega} = \frac{2}{\lambda_{\mathrm{opt}}} \int_{\omega_1}^{\omega_{\mathrm{m}}} \alpha^2 F(\omega) \omega d\omega, \text{(S13)}$$

For our predicted hydrides the $\lambda_{\mathrm{ac}} << \lambda_{\mathrm{opt}}$, we assume that:

$$T_c = T_c^{opt} + \Delta T_c^{ac}, \text{ and } {T_c}^{\mathrm{opt}} >> \Delta {T_c}^{\mathrm{ac}} \quad \text{(S14)}$$

As a result, the expression for $T_c$ can be written in the form:

$$T_c = \left[1 + 2 \frac{\lambda_{\mathrm{ac}}}{\lambda_{\mathrm{opt}} - \mu^*} \cdot \frac{1}{1+\rho^{-2}}\right] T_c^0, \rho = \frac{\widetilde{\omega}_{\mathrm{ac}}}{\pi T_c^0}, T_c^0 \equiv T_c^{opt}. \quad \text{(S15)}$$

Here the ${T_c}^0$ is defined as the transition temperatures caused by the interaction of electrons with optical phonons only; for $\lambda_{\mathrm{opt}} \leq 1.5$:

$$T_c^0 = \frac{\widetilde{\omega}_{\mathrm{opt}}}{1.2} \exp\left[-\frac{1.04(1+\lambda_{\mathrm{opt}})}{\lambda_{\mathrm{opt}} - \mu^*(1+0.62\lambda_{\mathrm{opt}})}\right]. \quad \text{(S16)}$$

For $\lambda_{\mathrm{opt}} > 1.5$:

$$T_c^0 = \frac{0.25\widetilde{\omega}_{\mathrm{opt}}}{[e^{\frac{2}{\lambda_{eff}}} - 1]^{1/2}}. \quad \text{(S17)}$$

Here the $\lambda_{\mathrm{eff}}$ is defined as follows:

$$\lambda_{\mathrm{eff}} = \left(\lambda_{\mathrm{opt}} - \mu^*\right)\left[1 + 2\mu^* + \lambda_{\mathrm{opt}} \mu^* t\left(\lambda_{\mathrm{opt}}\right)\right]^{-1}, \quad \text{(S18)}$$

$$t(x) = 1.5 \exp(-0.28x). \quad \text{(S19)}$$

The following expression:

$$\alpha = \frac{1}{2}\left[1 - 4 \frac{\lambda_{ac}}{\lambda_{opt}} \frac{\rho^2}{(\rho^2+1)^2}\right] \quad \text{(S20)}$$

allows us to calculate the isotope coefficient α.

## 8. Superconductive properties

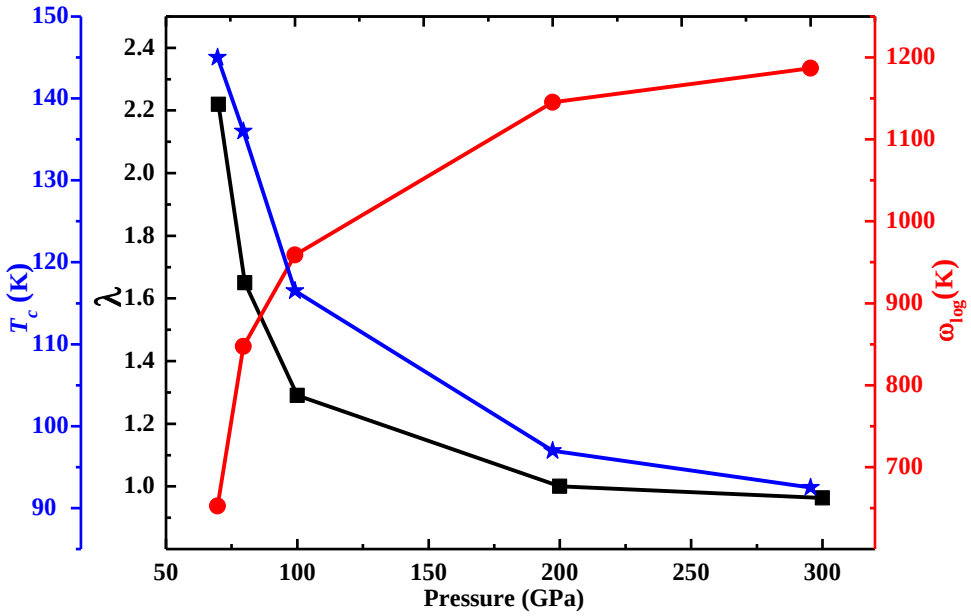


**Fig. S9.** The EPC parameter λ, logarithmic average frequency $\omega_{log}$, and $T_c$ of $YbH_6$ versus pressures.

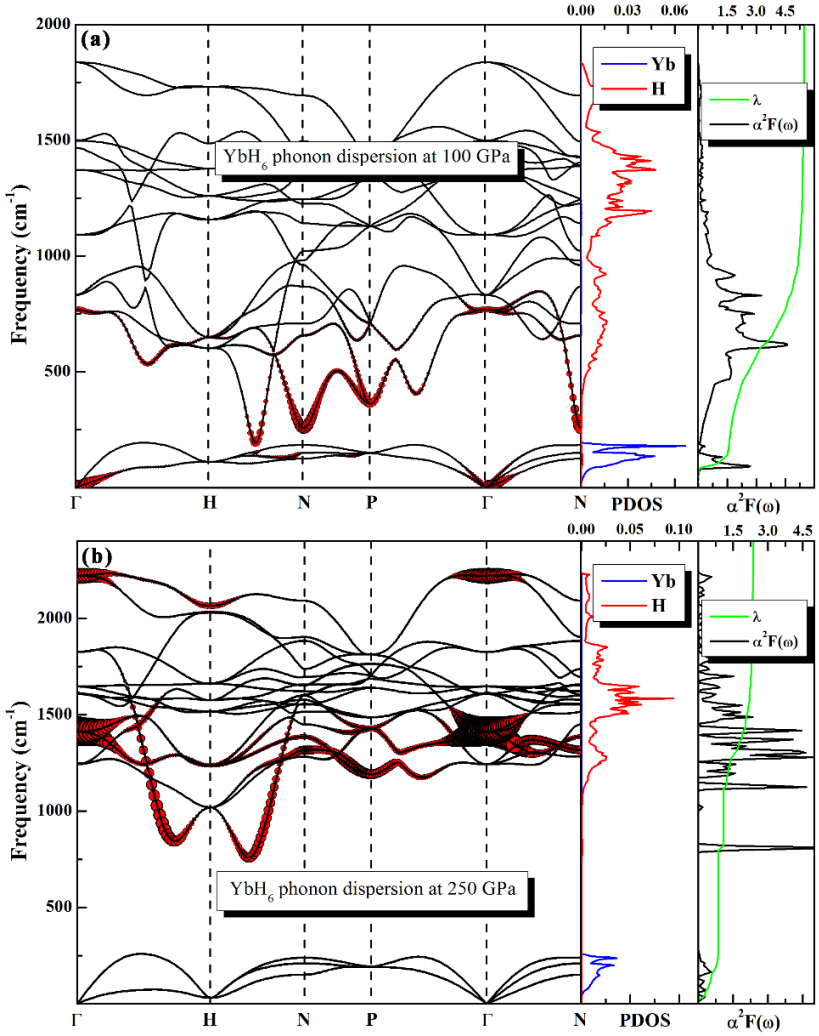


**Fig. S10.** Phonon dispersion, phonon density of state, spectral function ($\alpha^2F(\omega)$) and integral EPC λ of $Im\bar{3}m$-$YbH_6$ with frozen-*f* electrons at 100 GPa (a) and 250 GPa (b). Red circles with radius proportional to the EPC strength.

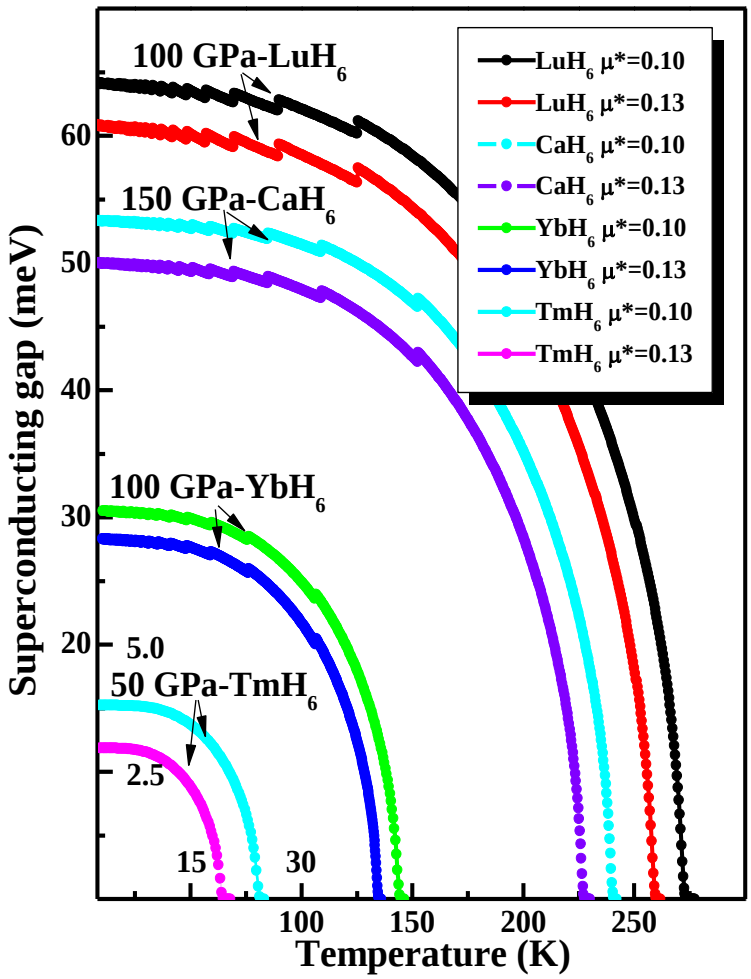


**Fig. S11.** The superconducting gap for $XH_6$ (X=Ca, Tm, Yb, Lu) at different pressure.

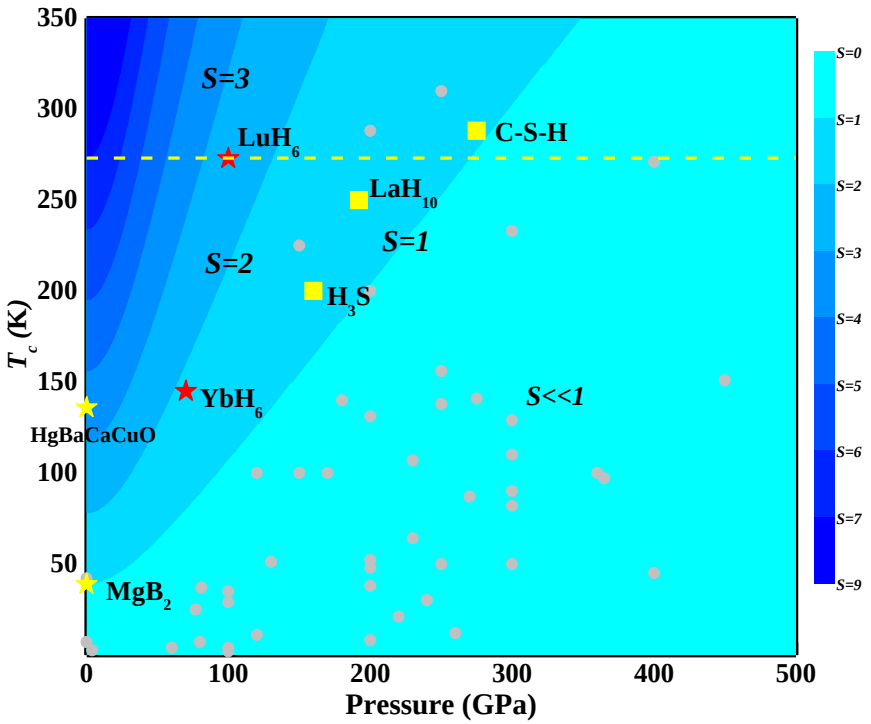


**Fig. S12.** The superconducting critical temperature $T_c$ as a function of the pressure for different hydrides. Small circles correspond to predictions as summarized in table 1 in [23]. Yellow stars represent $S(MgB_2) = 1$ and $S(HgBaCaCuO) = 3.5$, red stars represent $S(LuH_6) = 2.5$ and $S(YbH_6) = 1.8$ and yellow square represent $S(C\text{-}S\text{-}H) = 1.1$, $S(H_3S) = 1.3$ and $S(LaH_{10}) = 1.3$ [24]. The yellow dash-line represent ice point temperature. The colored contours correspond to the figure of merit $S = \frac{T_c}{\sqrt{T_{c,MgB_2}^2 + P^2}}, (T_{c,MgB_2} = 39\ \mathrm{K})$

**Table S3.** The calculated EPC parameter $\lambda$, logarithmic average phonon frequency $\omega_{log}$ (K), electronic density of states at Fermi level $N(\varepsilon_f)$ (states/spin/Ry/f.u.), isotope coefficients $\alpha$ and superconducting transition temperatures $T_c$ (K) with $\mu^*$=0.1-0.13 at corresponding pressures $P$ (GPa).

| Structure | $P$ | $\lambda$ | $\omega_{log}$ | $N(\varepsilon_f)$ | $\alpha$ | $T_c$ (K)[a] | Mc-A-D $T_c$ (K)[b] | AI $T_c$ (K) | G-K $T_c$ (K) |
|---|---|---|---|---|---|---|---|---|---|
| $Im\bar{3}m$ $YbH_6$ | 70 | 2.22 | 652.4 | 8.4 | 0.48 | 90-94 | 114-125 | 125-145 | 121-131 |
| | 100 | 1.29 | 959.0 | 7.6 | 0.44 | 83-93 | 87-101 | 99-116 | 98-102 |
| | 200 | 1.00 | 1146.5 | 6.8 | 0.38 | 69-80 | 72-85 | 82-96 | 78-91 |
| | 300 | 0.96 | 1186.9 | 6.4 | 0.35 | 65-77 | 69-80 | 77-92 | 72-87 |
| $Im\bar{3}m$ $LuH_6$ | 100 | 3.60 | 750.5 | 4.8 | 0.49 | 140-146 | 204-222 | 260-273 | 227-243 |
| | 200 | 1.77 | 1366.2 | 4.2 | 0.47 | 166-180 | 190-209 | 231-250 | 190-210 |
| $Im\bar{3}m$ $TmH_6$ | 50 | 0.72 | 611.9 | 29.6 | 0.47 | 17-22 | 18-23 | 19-24 | 19-25 |
| $Im\bar{3}m$ $EuH_6$ | 160 | 0.13 | 511.1 | 64.4 | \ | 0 | 0 | 0 | 0 |
| $Im\bar{3}m$ $CaH_6$ | 150 | 2.67 | 1027.1 | 2.4 | 0.38 | 165-175 | 205-222 | 227-241 | 220-236 |
| $Im\bar{3}m$ $YH_6$ | 120 | 3.06 | 829.0 | 4.7 | 0.46 | 143-150 | 195-213 | 244-257 | 218-234 |
| $Im\bar{3}m$ $H_3S$ | 200 | 1.88 | 1266.0 | 3.1 | 0.35 | 162-175 | 186-204 | 212-223 | 206-229 |

[a] $T_c$ was estimated using Allen-Dynes- McMillian equation with $f_1f_2 = 1$ (Eq. S1).

[b] $T_c$ was estimated using Allen-Dynes- McMillian equation with $f_1f_2 \neq 1$ (Eq. S2).

**Table S4.** The calculated EPC parameter $\lambda$, logarithmic average phonon frequency $\omega_{log}$ (K), electronic density of states at Fermi level $N(\varepsilon_f)$ (states/spin/Ry/f.u.) and superconducting transition temperatures $T_c$ (K) of $LuH_n$ (n=3,4,5,7) with $\mu^*$=0.1-0.13 at corresponding pressures $P$ (GPa).

| Structure | $P$ (GPa) | $\lambda$ | $\omega_{log}$(K) | $N(\varepsilon_f)$ | $T_c$ (K)[a] |
|---|---|---|---|---|---|
| $Fm\bar{3}m$ $LuH_3$ | 100 | 0.4 | 670 | 2.0 | 1-3 |
| $I4/mmm$ $LuH_4$ | 100 | 1.5 | 632 | 3.4 | 65-71 |
| $P4/nmm$ $LuH_5$ | 150 | 1.7 | 703 | 6.8 | 82-89 |
| $Cmc2_1$ $LuH_7$ | 150 | 0.6 | 1060 | 3.9 | 26-34 |

[a] $T_c$ was estimated using Allen-Dynes- McMillian equation with $f_1f_2$ = 1 (Eq. S1).

**Table S5.** The calculated $T_c$ of $XD_6$ (X=Yb, Lu, Y, Ca, and Sc) at different pressures.

| Parameter | $YbD_6$ | $LuD_6$ | $YD_6$ | $CaD_6$ | $ScD_6$ |
|---|---|---|---|---|---|
| | 70 GPa | 100 GPa | 120 GPa | 150 GPa | 300 GPa |
| $T_c^D$ (K) | 87-94 | 162-173 | 158-170 | 169-181 | 136-152 |

## References


[1] Pickard C J and Needs R J 2011. *J Phys Condens Matter* **23** 053201

[2] Pickard C J and Needs R J 2006. *Phys. Rev. Lett.* **97** 045504

[3] Segall M D, Lindan P J D, Probert M J, Pickard C J, Hasnip P J, Clark S J and Payne M C 2002. *J Phys Condens Matter* **14** 2717

[4] Payne M C, Teter M P, Allan D C, Arias T A and Joannopoulos J D 1992. *Rev. Mod. Phys.* **64** 1045

[5] Clark S J, Segall M D, Pickard C J, Hasnip P J, Probert M J, Refson K and Payne M C 2005. *Z. Kristallogr.* **220** 567

[6] Vanderbilt D 1990. *Phys. Rev. B* **41** 7892

[7] Perdew J P, Burke K and Ernzerhof M 1996. *Phys. Rev. Lett.* **77** 3865

[8] Monkhorst H J and Pack J D 1976. *Phys. Rev. B* **13** 5188

[9] Giannozzi P, Baroni S, Bonini N, Calandra M, Car R, Cavazzoni C, Ceresoli D, Chiarotti G L, Cococcioni M, Dabo I *et al.* 2009. *Journal of Physics  Condensed Matter* **21**

[10] Eliashberg G M 1960. *J. Exp. Theor. Phys.* **11** 696

[11] Allen P B and Dynes R C 1975. *Phys. Rev. B* **12** 905

[12] Bergmann G and Rainer D 1973. *Zeitschrift für Physik* **263** 59

[13] Rainer D and Bergmann G 1974. *J. Low Temp. Phys.* **14** 501

[14] Gor'kov L P and Kresin V Z 2018. *Rev. Mod. Phys.* **90** 16

[15] Klotz S, Casula M, Komatsu K, Machida S and Hattori T 2019. *Phys. Rev. B* **100** 5

[16] Olsen J S, Buras B, Gerward L, Johansson B, Lebech B, Skriver H L and Steenstrup S 1984. *Phys. Scr.* **29** 503

[17] Peng F, Sun Y, Pickard C J, Needs R J, Wu Q and Ma Y M 2017. *Phys. Rev. Lett.* **119** 6

[18] Wang H, John S T, Tanaka K, Iitaka T and Ma Y 2012. *Proc. Natl. Acad. Sci. U. S. A.* **109** 6463

[19] McMillan W L 1968. *Physical Review* **167** 331

[20] Dynes R C 1972. *Solid State Commun.* **10** 615

[21] Abrikosov A A, Gorkov L P and Dzyaloshinski I E, *Methods of quantum field theory in statistical physics* (Courier Corporation, 2012).

[22] Gor'kov L P and Kresin V Z 2016. *Sci. Rep.* **6** 25608

[23] Bi T, Zarifi N, Terpstra T and Zurek E 2019. *Reference Module in Chemistry, Molecular Sciences and Chemical Engineering*

[24] Pickard C J, Errea I and Eremets M I 2020. *Annu Rev Condens Matter Phys* **11** 57